Green tea extract coated magnetite nanoparticle as chimosensetive and hyperthermice responsive material

A. F. Aman [a,*], O. A. Ghazy [b], H. H. Saleh [b], I. A. Ali [c,d], N. H. Ahmed [e], S. A. Rizk [a], Z. I. Ali [b]

[a] *Chemistry Department, Faculty of Science, Ain Shams University. Cairo, Egypt*
[b] *Radiation Chemistry Department, National Center for Radiation Research and Technology (NCRRT), Egyptian atomic Energy Authority (EAEA), Cairo, Egypt*
[c] *Cyclotron Project, Nuclear Research Center, Egyptian Atomic Energy Authority (EAEA), Cairo, Egypt*
[d] *Nuclear Physics Department, Nuclear Research Center, Egyptian Atomic Energy Authority (EAEA), Cairo, Egypt*
[e] *Radiation Biology Department, National Center for Radiation Research and Technology, Egyptian Atomic Energy Authority (EAEA), Cairo, Egypt*

This study examines the synthesis and characterization of magnetite nanoparticles (Fe_3O_4 NPs) coated with green tea (GT) extract for cancer treatment. Two methods, In-Situ and Ex-Situ, were used for coating. TEM analysis showed size differences: In-Situ (5 ± 2 nm) and Ex-Situ (12 ± 3). FTIR and XRD confirmed nanocomposite formation. VSM analysis revealed higher saturation magnetization for Ex-Situ (37.10 emu/g) versus In-Situ (27.4 emu/g). Hyperthermia studies ranked magnetite > Ex- Fe_3O_4@GT > In- Fe_3O_4@GT in heating efficacy. Cell viability assays showed antitumor activity, with Ex-Situ samples responding faster and efficacy depending on Fe_3O_4@GT concentration against Ehrlich carcinoma cells.

(Received April 20, 2025; Accepted July 17, 2025)

Keywords: Magnetite nanoparticles, Green tea extract, Hyperthermia therapy, Fe_3O_4, Nanocomposites, Cell viability, Biomedical applications

1. Introduction

Magnetite nanoparticles (Fe_3O_4 NPs) have garnered substantial interest for their exceptional magnetic and physiochemical attributes, positioning them as versatile materials in versatile application and[1] biomedicine [2,3] Exhibiting superparamagnetic behaviour, characterized by a lack of residual magnetism and resistance to agglomeration in liquid mediums, these nanoparticles present an attractive feature for applications demanding stable dispersion and effortless magnetic separation [4]. In the realm of biomedicine, Fe_3O_4 NPs have found diverse utility, ranging from magnetic resonance imaging [5–7], and cell sorting to drug delivery [8], hyperthermia [9], tissue repair [10] , and the detoxification of biological fluids [11]. Their biocompatibility, coupled with the ease of surface coating and functionalization, has fuelled extensive research interest across various domains [12]. The synthesis of Fe_3O_4 NPs has undergone extensive exploration, utilizing conventional methods such as seed-mediated growth [13] , wet-chemical approaches [14] , and stepwise deposition [15], alongside more recent techniques like microwave-assisted [16] and spray pyrolysis [17] . However, the limitations inherent in many chemical synthesis routes, including the use of inorganic media and hydrophobic ligands, pose challenges for their widespread application in biomedical settings.

* Corresponding author: ch.ahmedmohmed@gmail.com
https://doi.org/10.15251/DJNB.2025.203.811

To overcome these challenges, researchers have turned to green synthesis methods employing natural extracts, with green tea emerging as a promising candidate. Green tea extract, enriched with polyphenolic compounds, particularly tea catechins, offers a spectrum of health benefits, including antioxidative, anticancer, anti-inflammatory, and antithrombogenic activities [18]. Additionally, the hydrophilic nature of green tea facilitates enhanced stability and dispersion of the nanoparticles in aqueous media, critical for their biomedical applications [19].Magnetic hyperthermia using magnetite (Fe_3O_4) nanoparticles is a promising cancer treatment. These superparamagnetic nanoparticles convert alternating magnetic fields (AMFs) into localized heat through hysteresis and relaxation, raising tumor temperatures to 41-45 °C. This induces cancer cell stress and apoptosis while sparing healthy tissues. Functionalizing Fe_3O_4 nanoparticles with targeting ligands enhances tumor specificity. Challenges include optimizing nanoparticle size, magnetic properties, and tumor distribution, controlling heat depth, ensuring biocompatibility, and minimizing toxicity. Advancing this approach requires ongoing research and clinical trials, with material scientists driving progress toward effective, minimally invasive treatments [20].This study aims to bridge synthesis methodologies with potential biomedical applications, advancing our understanding of these nanocomposites in cancer treatment. It builds on the work of Xiao et al. (2015), who demonstrated the synthesis of green tea-coated, water-soluble Fe_3O_4 magnetic nanoparticles [21]. Our investigation takes this further by focusing on the synthesis and characterization of magnetite loaded with green tea extract using two distinct methods: in-situ and ex-situ synthesis. Additionally, we explored the potential of the resulting materials as hyperthermia-responsive agents. The chemosensitivity of the nanocomposites was also evaluated by assessing their impact on the viability of Ehrlich ascites carcinoma cells using the trypan blue dye assay.

2. Experimental work

2.1. Materials

The following reagents were used in the preparation: Iron (III) chloride hexahydrate ($FeCl_3 \cdot 6H_2O$, 99% w/w; Merck), iron (II) sulfate heptahydrate ($FeSO_4 \cdot 7H_2O$, 99% w/w; Merck), green tea leaves, and ammonium hydroxide solution (NH_4OH, 30 wt%).

2.2. Preparation of green tea extract

Green tea leaves were thoroughly rinsed three times with double-distilled water. Following this, two separate batches were prepared by adding 0.5 g and 1.0 g of green tea leaves to 100 mL of deionized water in separate beakers. These mixtures were boiled in a water bath for 15 minutes, then allowed to cool to room temperature. After cooling, the extracts were filtered using Whatman filter paper No. 1 to obtain the aqueous solutions. The resulting extracts, corresponding to 0.5 g and 1.0 g of leaves, were designated as Extract 1 and Extract 2, with concentrations of 5 mg/mL and 10 mg/mL, respectively.

2.3. Preparation of Fe_3O_4@GT nanocomposites (ex-situ method)

Fe_3O_4 nanoparticles (NPs) were synthesized by dissolving 0.66 g of $FeCl_3 \cdot 6H_2O$ and 0.33 g of $FeSO_4 \cdot 7H_2O$ in 80 mL of deionized water. This solution was de-aerated by ultrasonication for approximately 15 minutes to remove dissolved oxygen. While stirring at 50°C, 30% ammonia solution was rapidly added to adjust the pH to 10, resulting in the formation of an iron hydroxide suspension. The solution was then divided into two separate beakers.In the first beaker, 20 mL of Extract 1 (5 mg/mL) was added, while 20 mL of Extract 2 (10 mg/mL) was added to the second beaker. Both solutions were stirred continuously, leading to the formation of black colloidal suspensions, which indicated the successful coating of Fe_3O_4 nanoparticles with green tea extract (Fe_3O_4@GT). The suspensions were left to age overnight to enhance the coating stability. Following this, the nanoparticles in each beaker were separated via magnetic decantation, washed sequentially with deionized water and ethanol, and then vacuum-dried at 50 °C overnight [22] . The resulting samples were labeled as Ex-Fe_3O_4@GT1 and Ex-Fe_3O_4@GT_2, corresponding to the nanoparticles synthesized with Extract 1 and Extract 2, respectively. Additionally, uncoated Fe_3O_4 NPs were prepared under similar conditions for comparative purposes and labeled as Fe_3O_4.

2.4. Preparation of Fe_3O_4@GT nanocomposites (in-situ method)

For the in-situ synthesis, two separate beakers were prepared to allow for the distinct addition of Extracts 1 and 2. In the first beaker, 0.66 g of $FeCl_3 \cdot 6H_2O$ and 0.33 g of $FeSO_4 \cdot 7H_2O$ were combined with Extract 1 (5 mg/mL), maintaining a molar ratio of Fe^{3+}: Fe^{2+} at 2:1. Similarly, in the second beaker, the same quantities of FeCl3·6H2O and FeSO4·7H2O were combined with Extract 2 (10 mg/mL).

Both mixtures were chemically precipitated at 40°C by the dropwise addition of 30% ammonium hydroxide under vigorous stirring. Following precipitation, the temperature of each solution was raised to 50°C and maintained for 1 hour under continuous stirring to facilitate nanoparticle formation. The resultant Mag@GT nanoparticles were isolated using an external magnet, rinsed with deionized water, and vacuum-dried at 40°C [23].These samples were labeled as In-Fe_3O4@GT_1 and In-Fe_3O^4@GT_2, representing the nanoparticles synthesized with Extract 1 and Extract 2, respectively.

2.5. Characterization

The nanocomposites generated in this study underwent thorough characterization utilizing diverse techniques to elucidate their structural and magnetic properties.

2.5.1. Fourier transform infrared spectroscopy (FTIR)

Fourier transform infrared spectra were acquired employing a Unicam England FT-IR model Mattson-Genssis, spanning the range of 4000-400 cm^{-1}. This analysis aimed to unravel the chemical composition and functional groups present in the nanocomposites.

2.5.2. High-resolution transmission electron microscopy (HR-TEM)

High-resolution transmission electron microscopy (HR-TEM) utilizing a JEOL-JEM-200CX instrument was employed to validate the nano-size and shape of the prepared nanocomposites. This technique provides detailed insights into the morphology at the nanoscale.

2.5.3. X-ray diffraction (XRD)

X-ray diffraction patterns were collected utilizing a Bruker D2 Advance instrument equipped with Cu Kα radiation (λ = 1.5406 Å). This analysis delved into the crystallographic properties of the nanocomposites, elucidating their structural characteristics.

2.5.4. Vibrating-sample magnetometer (VSM)

The magnetic properties of the nanocomposites were scrutinized through vibrating-sample magnetometer (VSM) measurements conducted using a LAKESHORE Cryotronic 7400-S instrument. This investigation aimed to quantify the saturation magnetization, offering insights into the magnetic behavior of the nanocomposites.

This comprehensive characterization approach allows for a holistic understanding of the prepared nanocomposites, providing crucial data on their structural, chemical, and magnetic attributes. The amalgamation of these results contributes to the elucidation of the nanocomposites' potential applications in various fields, particularly in the realms of biomedical and material science.

2.6. Cell viability by trypan blue dye assay

In Vitro Study - Chemosensitivity of Nanoparticles (Cell Viability)

The antitumor effect of nanoparticles was evaluated by observing changes in viable and nonviable tumor cell counts. Cytotoxicity effects on tumor cells were determined following the method of Shete et al. (2014) [24] . Ehrlich ascites carcinoma cells (EACs) were treated with nanoparticles at concentrations ranging from 10 to 100 µg/ml. EACs were obtained through needle aspiration of ascites fluid from reinoculated mice under aseptic conditions using an ultraviolet laminar airflow system. Percentages of non-viable cells were determined by counting dead and viable EACs using trypan blue stain. The formula % NVC = C/T × 100, where C is the number of non-viable cells and T is the total number of viable cells, was employed for quantification. This assay provided insights into the cytotoxic impact of Fe_3O_4@GT Polyphenols Fe_3O_4GTPs NPs on

Ehrlich ascites carcinoma cells, paving the way for a comprehensive understanding of their potential applications in cancer treatment.

2.7. Hyperthermia

A suspension solution was prepared using the ball milling method, we synthesized a colloidal suspension from 1.0g of pre-made nanocomposites and MilliQ water. The milling process was performed at 1000 rpm for 30 minutes with a 2:1 on-off cycle. After milling, the suspension was filtered and stored below 20 °C to maintain its volume. This process ensures a high-quality nanocomposite suspension for further use. The resulted solution exposed to the field using an induction heater and the resulting temperature profiles were analyzed. Following dispersion in MilliQ water via sonication for 15 minutes and centrifugation at 12500 r.p.m for 30 minutes to remove unreacted chemicals. Then Fe_3O_4@Cs nanocomposites were resuspended in MilliQ water and subjected to hyperthermia treatment, where an induction heater DW-UHF-10 kW (China) with a coupling coefficient (H) of 9.27 $kA \cdot m^{-1}$ was employed to investigate the temperature rise of the suspension at a fixed frequency of 198 kHz. The suspension was housed within a Pyrex tube and inserted into the water-cooled copper coil of the heater. A digital infrared thermometer (UNI-T: UT305A) was utilized to monitor the temperature increase of the sample.

3. Results and discussion

3.1. Nanocomposite morphology and structure

High resolution transmission electron microscopy (HR-TEM) micrographs of pure Fe_3O_4 (a) and Ex-Fe_3O_4@GT (b, c) and In-Fe_3O_4@GT (d, e) nanocomposites revealed distinctive morphologies, as depicted in Fig. 1. The nano-sized morphology of Fe_3O_4 @GT, observed in Fig. 1 (b,c) highlighted the impact of Green Tea (GT) incorporation, resulting in size reduction and distinct polygonal and hexagonal shapes during the in-situ preparation route. HR-TEM measurements indicated average sizes of 10 ± 2 nm for pure Fe_3O_4, 12 ± 3 nm for both Ex- Fe_3O_4@GTs Fig. 1 (b,c), and 5 ± 2 nm for In- Fe_3O_4@GTs, Fig. 1 (d,e). The increase in particle size of Ex- Fe_3O_4@GTs from 10 nm to 12 nm after exposure to green tea extract is likely due to the formation of an organic coating from polyphenols and other compounds in the extract. This coating stabilizes the nanoparticles by providing a thin protective layer, and enhance their dispersibility [25].

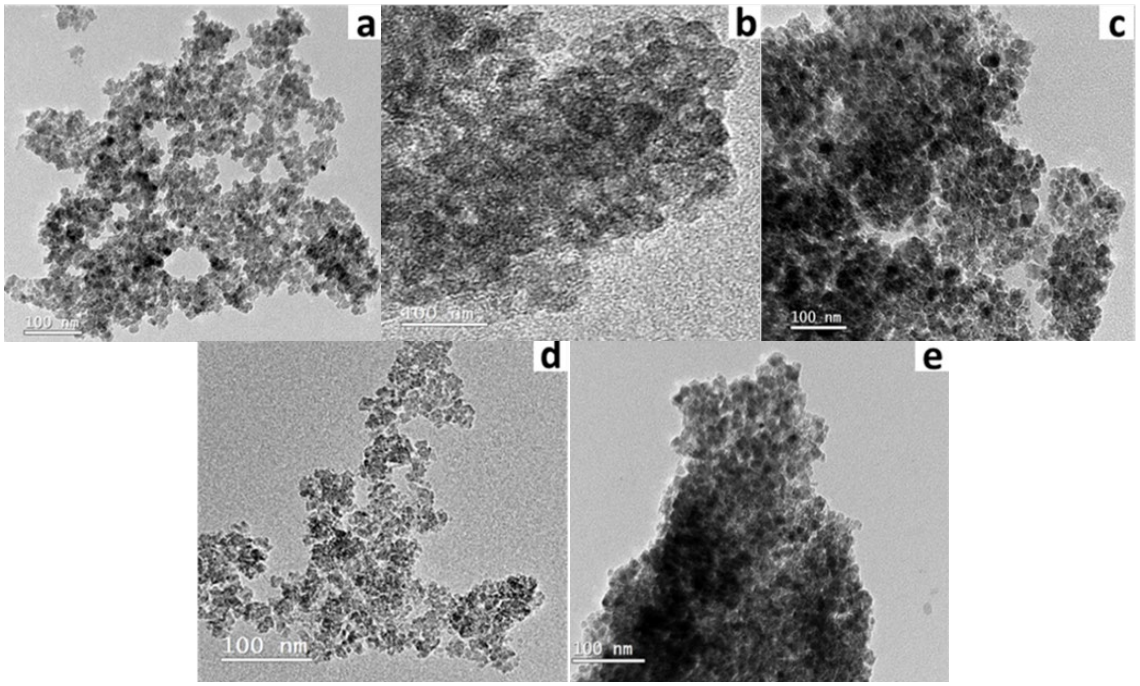

Fig. 1. HE-TEM micrographs of (a) Pure magnetite particles (b) Ex-Mag@GT_1 (c) Ex-Mag@GT_2, (d) In-Fe_3O_4@GT_1 and (e) In-Fe_3O_4@GT_2.

The agglomeration of nanoparticles, evidenced by Fig. 1 (b to e), can be attributed to inter-hydrogen bonding interactions between magnetite and GT functional groups and Intra-hydrogen bonding interactions between GT functional groups in different nanoparticles [26] .

3.2. FTIR analysis

Verification of characteristic functional groups in GT extract and Fe3O4 nanoparticles through FTIR analysis. The FTIR spectra of pure Fe_3O_4 and Fe_3O_4@GT nanocomposites, incorporating different extract concentrations of GT, are presented in Fig. 2 a. notably, the FTIR spectra of pure Fe_3O_4. nanoparticles show a prominent and broad band at approximately 555 cm-[122] , corresponding to the Fe–O bond which did not suffer any shift for both Fe_3O_4@GT nanocomposites as well as the bending OH band at 1622 cm-1 and stretching OH at 3350 cm-1 a study done by Huang et al came to the same result [27] . The bands of the OH groups were attributed to the phenolic compounds in GT extract [28] The In-Fe_3O_4@GT and Ex-Fe_3O_4@GT nanocomposites share common peaks corresponding to GT such as peaks at 1054, which are ascribed to amino C-O, amid-I protein, C-N stretching vibrations at 1251 cm-1 while at 1396 cm-1 stretching C=C in GT[21] . GT carboxylic acids exhibit two stretching vibrations at 2895 and 2990 cm-1 due to the presence of C-H and O-H groups in case of In-Fe_3O_4@GT samples [29] . These two peaks disappeared in Ex-Fe_3O_4 @GT samples giving an indication that they are the adsorption sites on the surface of Fe_3O_4 Nanoparticles after mixing. Furthermore, Ex-Fe_3O_4@GT2 has an extra peak at 1145 cm-1 corresponding to C-O stretching in aliphatic ether. The absence of such peak in In-Fe_3O_4@GT samples can be due to the strong adsorption of GT on the surface of Fe_3O_4 nanoparticles during the In-Situ preparation. [28–30]

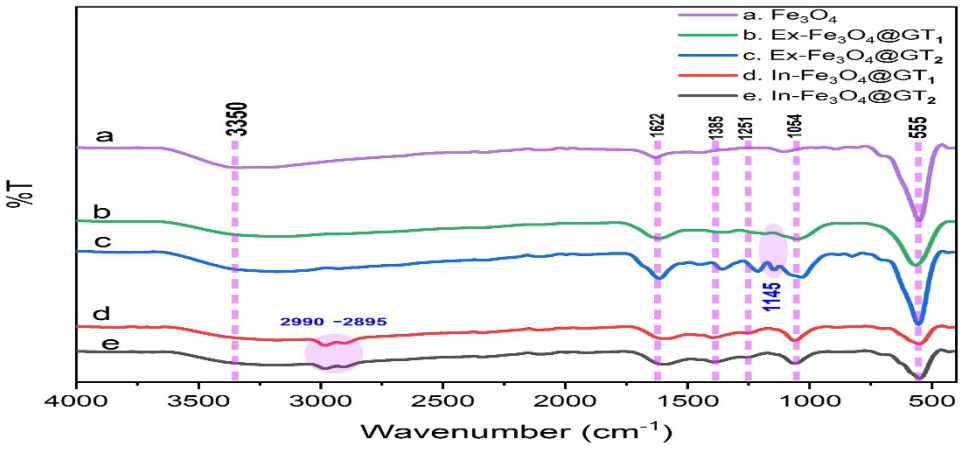

Fig. 2. FTIR spectra of (a) Pure Fe_3O_4 particles (b) Ex-Mag@Cs_1 (c) Ex-Mag@Cs_2, (d) I In-Fe_3O_4@GT_1 and (e) In-Fe_3O_4@GT_2.

FTIR analysis validated the stability of Fe_3O_4 nanoparticles after GT mixing. Variances between In-Fe_3O_4@GT and Ex-Fe_3O_4@GT samples, including the disappearance of specific peaks in the two Ex-Fe_3O_4@GT samples, suggested distinct adsorption dynamics during In-Situ and Ex-Situ preparations.

3.3. X-Ray diffraction (XRD) analysis

The crystallographic properties of Fe_3O_4@GT nanocomposites were comprehensively investigated using X-ray diffraction (XRD) analysis. The XRD patterns exhibited a combination of peaks corresponding solely to Fe_3O_4 nanoparticles, with slight deviations in their positions. The peaks of pure Fe3O4 were characterized by distinct angles at 2θ of 30.08°, 35.42°, 43.08°, 53.56°, 56.98°, and 62.62°, corresponding to the Miller indices (220), (311), (400), (422), (511), and (440), respectively (Fig. 3) which is in accordance to(ICDD card number 19-629 [23] . In the XRD patterns of Ex-Fe_3O_4@GT (Fig. 3b) and In- Fe_3O_4@GT (Fig. 3c), the reflection planes displayed broadening,

accompanied by changes in peak intensities, which is indicative of the reduced crystal size of the magnetic particles [31].

Crystal structure analysis of Ex-Fe_3O_4@GT revealed broadening and slight shift towards smaller angles, suggesting alterations in the Fe3O4 crystal structure resulting from surface adsorption of GT extract on Fe_3O_4 [32]. The broadening and dimensioning observed in the In-Fe_3O_4@GT peaks indicate that the in-situ synthesis process resulted in the formation of Fe_3O_4 nanoparticles with less crystalline structure. In addition, the in-situe synthesis was expected to provide thicker coating layer on the surface of Fe_3O_4 nanoparticles. These findings provide valuable insights into the structural attributes of Fe_3O_4@GT nanocomposites and elucidate the influence of GT extract on the crystallinity and morphology of the resulting materials [33]

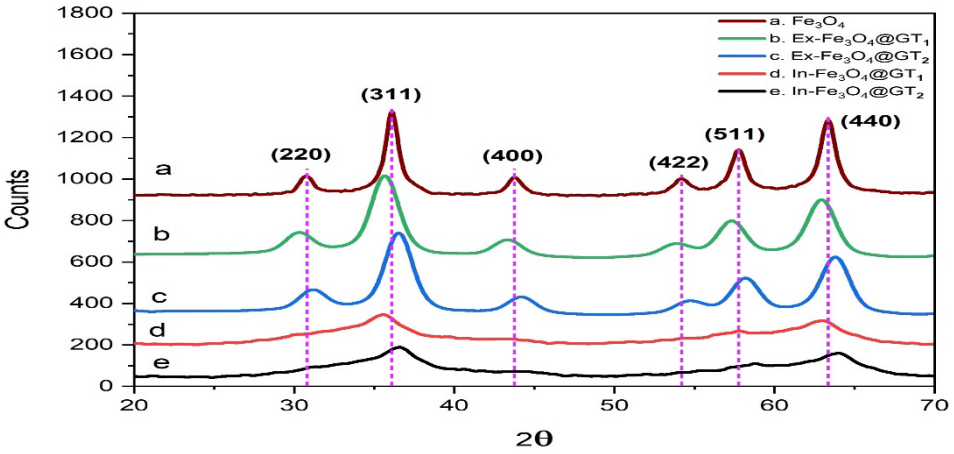

Fig. 3. XRD patterns of spectra of (a) Pure Fe_3O_4 nanoparticles (b) Ex-Mag@GT_1 (c) Ex-Mag@GT_2, (d) In-Fe_3O_4@GT1 and (e) In-Fe_3O_4@GT_2.

3.4. Magnetic properties

Magnetic properties were investigated via vibrating sample magnetometer (VSM); (Fig. 4). The values of the saturation magnetization (MS) at room temperature for different samples were listed in Table 1.

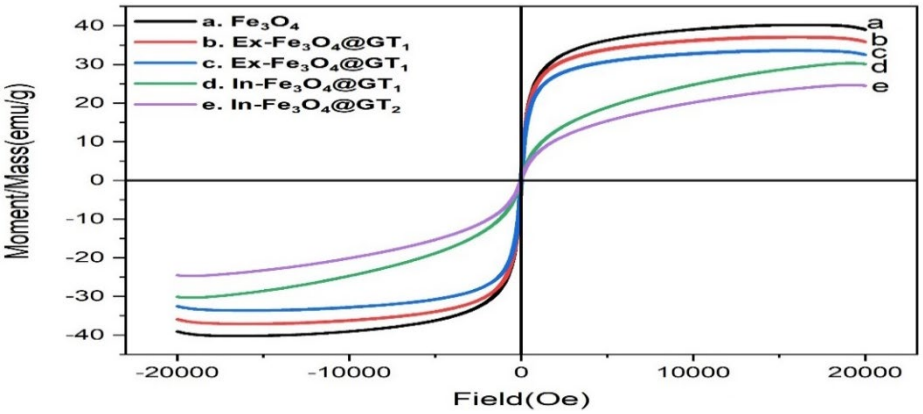

Fig. 4. VSM of (a) Fe_3O_4 (b) Ex- Fe_3O_4@GT_1, (c) Ex- Fe_3O_4@GT_2, (d) In- Fe_3O_4 @GT_1 and (e) In-Fe_3O_4@GT_2.

Table 1. The saturation magnetization values (Ms) of pure Fe_3O_4 nanoparticles, Ex-Fe_3O_4@GT and In-Fe_3O_4@GT samples.

Sample	Fe_3O_4	Ex-Fe_3O_4@GT_1	Ex-Fe_3O_4@GT_2	In-Fe_3O_4@GT_1	In-Fe_3O_4@GT_2
Ms	40.2	37.1	33.5	30.33	24.7

The observed results suggest the presence of superparamagnetic behavior in the nanoparticles. The order of the MS values is pure Fe_3O_4 nanoparticles > Ex-Fe_3O_4@GT_1 > Ex-Fe_3O_4@GT_2 > In-Fe_3O_4@GT_1 > In-Fe_3O_4@GT_2 (Table 1). Consequently, the Fe_3O_4 and Ex-Fe_3O_4@GT samples achieve magnetic saturation more rapidly than the In-Fe_3O_4@GT samples. This difference is likely attributable to variations in surface modifications and magnetic domain interactions, compounded by the smaller size of the In-Fe_3O_4@GT nanoparticles [34,35] . The results indicate that the synthesis procedure as well as the concentration of the GT extract highly affect the magnetic properties of the Fe_3O_4 nanoparticles [36–38]

3.5. Hyperthermia

Our study investigates the hyperthermic efficacy of Fe_3O_4@GT nanocomposites by evaluating their thermal response when subjected to an alternating magnetic field, as explained by Laurent S. et al (2011) [39]. All specimens demonstrated a consistent initial temperature increase, as depicted in (Fig. 5) The trend of maximum temperature elevation was as follows: pure Fe_3O_4 Nanoparticles > Ex- Fe_3O_4@GT1 > Ex- Fe_3O_4@GT2 > In- Fe_3O_4@GT1 > In- Fe_3O_4@GT2, Table 2. The results reveald that the samples prepared via the ex-situ method had higher hyperthermic response to the magnetic field. In addition, the higher concentration of GT extract caused a slight decrease in the hyperthermic response. However, all samples exhibited a final temperature higher than 41 °C, which is the recommended temperature for hyperthermia therapeutic treatment [40].

The trend of the hyperthermic response of the samples correlates well with the magnetic characterization results (Table 1), underscoring the potential of Ex-Fe_3O_4@GT nanocomposites for hyperthermia therapy. The disparate heating efficiencies observed can be ascribed to the impact of particle size reduction on the magnetic attributes of the materials, which is in concordance with the (VSM) analysis. Also, the rate of gain in temperature (Table 2) it was obvious in VSM Figure 4 that the In- Fe_3O_4@GT samples has the lowest retentivity and the longest magnetic saturation times which delayed their hyperthermia effect than Ex- Fe_3O_4@GT.

It is imperative to conduct further research to refine the composition and structure of these composites, aiming to realize precise and regulated hyperthermia in biologically pertinent settings. Various studies have explored hyperthermia applications using Fe_3O_4 nanoparticles, demonstrating diverse temperature ranges, concentrations, and durations. Zayed et al [41]. reported 43°C at 1 g/L in 20 minutes, while Karade et al [42]. recorded 43–45°C at 10 and 5 µg/mL in 6–10 minutes, reaching 40°C in 6 minutes. Sarma et al [43]. maintained 43°C at 5 mg/mL over 15 minutes, and observed 32°C, 39°C, and 50°C at concentrations of 3, 6, and 9 mg/mL within 550 seconds. This work achieved temperatures of 42.3–50.2 °Cat concentrations of 5 and 10 mg/mL within 400 seconds.

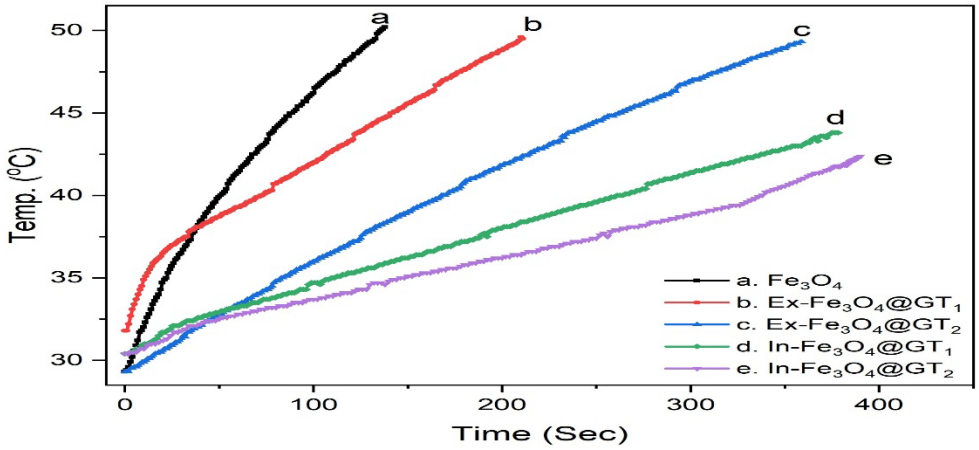

Fig. 5. Temperature profile with time for alternating magnetic fields at 198 kHz for (a) Magnetite, (b) Ex-Fe_3O_4@GT1 (c) Ex-Fe_3O_4@GT_2, (d) In-Fe_3O_4@GT_1 and (e) In-Fe_3O_4@GT_2.

These findings highlight variability in temperature and time parameters across studies, reflecting differences in synthesis methods and experimental conditions.

Table 2. Final temperature reached after 400 seconds of exposing to applied magnetic field.

Fe_3O_4@GT	Pure Fe_3O_4	Ex- Fe_3O_4@GT_1	Ex- Fe_3O_4@GT_2	In- Fe_3O_4@GT_1	In- Fe_3O_4@GT2
Final Temp (°C).	50.2	49.5	49.3	43.8	42.3
Rate of gain in Temp.*	0.14219 ± 0.00193	0.07166 ± 4.12871E-4	0.05601 ± 2.11222E-4	0.03399 ± 9.38726E-5	0.02816 ± 1.63946E-4

* Measured from the linear fitting of temperature profile vs time

3.6. Cell viability

In vitro studies assessed the antitumor effect of EX-Fe_3O_4@GT and In- Fe_3O_4@GT samples by investigating thier . cytotoxicity effects on Ehrlich ascites carcinoma cells through trypan blue dye assay. The obtained data were presented in Table 3. Ex-Situ Fe_3O_4@GT1 sample showed a cytotoxic effect starting from 30 µg/ml, while In-Situ Fe_3O_4@GT1 sample exhibited shrinkage effects on cells from 30 to 90 µg/ml.The observed cytotoxic effects underscore the potential of Fe_3O_4@GT Polyphenols NPs in tumor cell inhibition. Variations between Ex-Situ and In-Situ preparations suggest distinct interactions with tumor cells, emphasizing the importance of synthesis approaches in influencing biological responses. These findings hold promise for the development of effective cancer treatment modalities [21,39,44]

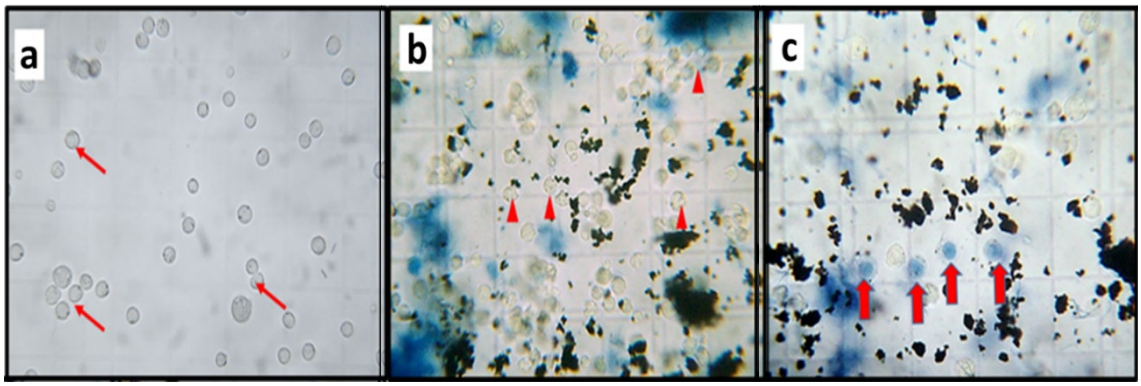

Fig. 5. Photomicrograph recording Ehrlich ascites carcinoma cells as effected by Ex-Fe_3O_4@GT: (a) Normal viable Ehrlich ascites carcinoma cells (↑), (b) Shrinkage Ehrlich ascites carcinoma cells (▲) and (c) Dead Ehrlich ascites carcinoma cells (⬆).

Table 3. The effect of Ex-Fe_3O_4@GT and In-Fe_3O_4@GT on the viability of Ehrlich ascites carcinoma cells (ECs).

Ex-Fe_3O_4@GT1 sample		
concentration (µg/mL)	% of viable cells	% of dead cells
0	100	-
9	100	-
10	100	-
20	100	-
30	-	Most of the ECs were shrunk
40	-	Most of the ECs were shrunk
50	-	Most of the ECs were shrunk
60	-	Most of the ECs were shrunk
70	-	Most of the ECs were shrunk
80	-	Most of the ECs were shrunk
90	-	Most of the ECs were shrunk
100	-	Most of the ECs were shrunk + 30 % dead
In-Fe_3O_4@GT1 Sample		
concentration (µg/mL)	% of viable cells	% of dead cells
0	100	-
9	100	-
10	100	-
20	100	-
30	-	Most of the ECs were shrunk
40	-	Most of the ECs were shrunk
50	-	Most of the ECs were shrunk
60	-	Most of the ECs were shrunk
70	-	Most of the ECs were shrunk
80	-	Most of the ECs were shrunk
90	-	Most of the ECs were shrunk
100	-	Most of the ECs were shrunk

The study revealed no decrease in tumor cell viability at lower concentrations (10 and 20 µg/ml), indicating low cytotoxicity. However, a gradual cytotoxic effect was observed from 30 up to 90 µg/ml, leading to cell shrinkage and eventual death, suggesting a controlled antitumor response. This progressive effect minimizes abrupt adverse reactions but may result in a delayed therapeutic response. At higher concentrations (30 to 100 µg/ml), the cytotoxic impact was more pronounced, with ascites cells showing prompt shrinkage and death. While this indicates effective tumor targeting at higher doses.

4. Conclusion

Magnetite nanoparticles (Fe_3O_4) were coated with green tea extract through either In-Situ or Ex-Situ methods. Comprehensive characterization employing HR-TEM, VSM, XRD, and FTIR spectral studies elucidated the distinctive features of the prepared nanocomposites. In the In-Situ synthesis, the resultant nanocomposites exhibited a reduced size range of 5 ± 2 nm, in contrast to the Ex-Situ counterparts with a larger size range of 12 ± 3 nm. This difference resulted in a lower magnetism for the In-Situ-synthesized nanocomposites. This effect was obvious in the hyperthermic response, where the Ex-situ prepared nanocomposites exhibited higher hyperthermic response than the In-situ prepared samples. The cytotoxicity test on Ehrlich ascites carcinoma cells demonstrated that samples prepared by both synthesis methods exhibited a comparable behavior where a dose of 30 µg/ml of either was adequate to cause cell shrinkage. Both the Ex-situ and In-situ synthesis methods provided nanocompsite materials that can be applied for the hyperthermic application.

Acknowledgments

We extend our sincere gratitude to Professor Maher El-Hashash for his dedication and for providing the foundational research direction for this study. Furthermore, we acknowledge the distinguished collaboration between the Faculty of Science, Ain Shams University, and the Egyptian Authority for Nuclear Research, which greatly contributed to the success of this work.

References

[1] Munoz, M., de Pedro, Z. M., Casas, J. A., Rodriguez, J. J., Appl Catal B 176-177, 249-265 (2015); https://doi.org/10.1016/j.apcatb.2015.04.003

[2] Lee, N. et al., Chem Rev 115, 10637-10689 (2015); https://doi.org/10.1021/acs.chemrev.5b00112

[3] Ling, D., Hyeon, T., Small 9, 1450-1466 (2013); https://doi.org/10.1002/smll.201202111

[4] Rui Hao, B. et al., Advanced Materials 22, 2729-2742 (2010); https://doi.org/10.1002/adma.201000260

[5] Tiefenauer, L. X., Tschirky, A., Kühne, G., Andres, R. Y., Magn Reson Imaging 14, 391-402 (1996); https://doi.org/10.1016/0730-725X(95)02106-4

[6] Owen, C. S., Sykes, N. L. J Immunol Methods 73, 41-48 (1984); https://doi.org/10.1016/0022-1759(84)90029-2

[7] Ntv, A., Chau, N. Applications of magnetite nanoparticles for water treatment and for DNA and cell separation. (2008).

[8] Yew, Y. P. et al., Arabian Journal of Chemistry 13, 2287-2308 (2020); https://doi.org/10.1016/j.arabjc.2018.04.013

[9] Ito, A., Honda, H., Kobayashi, T., Cancer Immunology, Immunotherapy 55, 320-328 (2006); https://doi.org/10.1007/s00262-005-0049-y

[10] Dasari, A., Xue, J., Deb, S., Nanomaterials 2022, Vol. 12, Page 757 12, 757 (2022); https://doi.org/10.3390/nano12050757

[11] Lattuada, M. et al., J Mater Chem B 4, 7080-7086 (2016); https://doi.org/10.1039/C6TB01272H

[12] Zhen Li, B. et al. One-Pot Reaction to Synthesize Biocompatible Magnetite Nanoparticles** ± [*] Prof.; https://doi.org/10.1002/adma.200401545

[13] Martínez-Mera, I., Espinosa-Pesqueira, M. E., Pérez-Hernández, R., Arenas-Alatorre, J., Mater Lett 61, 4447-4451 (2007); https://doi.org/10.1016/j.matlet.2007.02.018

[14] Sun, S., Zeng, H., J Am Chem Soc 124, 8204-8205 (2002); https://doi.org/10.1021/ja026501x

[15] Petcharoen, K., Sirivat, A., Materials Science and Engineering: B 177, 421-427 (2012); https://doi.org/10.1016/j.mseb.2012.01.003

[16] Daou, T. J. et al., Chemistry of Materials 18, 4399-4404 (2006); https://doi.org/10.1021/cm060805r

[17] Strobel, R., Pratsinis, S. E., Advanced Powder Technology 20, 190-194 (2009); https://doi.org/10.1016/j.apt.2008.08.002

[18] Sci-Hub, Materials Research Express, 4(9), 096102; https://doi.org/10.1088/2053-1591/aa892f

[19] Shahrashoub, M., Bakhtiari, S., Afroosheh, F., Googheri, M. S., Colloids Surf A Physicochem Eng Asp 622, 126675 (2021); https://doi.org/10.1016/j.colsurfa.2021.126675

[20] Salmanian, G., Hassanzadeh-Tabrizi, S. A., Koupaei, N., Int J Biol Macromol 184, 618-635 (2021); https://doi.org/10.1016/j.ijbiomac.2021.06.108

[21] Xiao, L. et al., ACS Appl Mater Interfaces 7, 6530-6540 (2015); https://doi.org/10.1021/am508404t

[22] Nie, L. et al., Curr Nanosci 17, 646-657 (2020); https://doi.org/10.2174/1573413716999201029205654

[23] Choi, K. H. et al., Journal of Physical Chemistry C 115, 3212-3219 (2011); https://doi.org/10.1021/jp1085137

[24] Shete, P. B. et al., Appl Surf Sci 288, 149-157 (2014); https://doi.org/10.1016/j.apsusc.2013.09.169

[25] Pattanayak, M., Mohapatra, D. & Nayak, P. L., Journal of Scientific Research 8, 184-187 (2013).

[26] Talbot, D. et al., ACS Omega 6, 19086-19098 (2021); https://doi.org/10.1021/acsomega.1c02401

[27] Huang, L., Weng, X., Chen, Z., Megharaj, M., Naidu, R., Spectrochim Acta A Mol Biomol Spectrosc 117, 801-804 (2014); https://doi.org/10.1016/j.saa.2013.09.054

[28] Carvalho, D. G., Ranzan, L., Jacques, R. A., Trierweiler, L. F., Trierweiler, J. O. Microchemical Journal 169, 106570 (2021); https://doi.org/10.1016/j.microc.2021.106570

[29] Irshad, S. et al., Cogent Chem 4, 1469207 (2018); https://doi.org/10.1080/23312009.2018.1469207

[30] Jiang, W. et al., Nanoscale 6, 1305-1310 (2014); https://doi.org/10.1039/C3NR05003C

[31] Holder, C. F., Schaak, R. E., ACS Nano 13, 7359-7365 (2019); https://doi.org/10.1021/acsnano.9b05157

[32] Giannini, C. et al., Crystals 2016, Vol. 6, Page 87 6, 87 (2016); https://doi.org/10.3390/cryst6080087

[33] Yang, X. et al., J Magn Magn Mater 324, 2249-2257 (2012); https://doi.org/10.1016/j.jmmm.2012.02.111

[34] Vestal, C. R., Zhang, Z. J., J Am Chem Soc 125, 9828-9833 (2003); https://doi.org/10.1021/ja035474n

[35] Liu, H., Chen, W., RSC Adv 5, 27034-27042 (2015); https://doi.org/10.1039/C5RA00985E

[36] Filippousi, M. et al., Journal of Physical Chemistry C 118, 16209-16217 (2014); https://doi.org/10.1021/jp5037266

[37] Sun, X. et al., Journal of Physical Chemistry C 112, 17148-17155 (2008); https://doi.org/10.1021/jp805724s

[38] Liu, C., Zhang, Z. J., Chemistry of Materials 13, 2092-2096 (2001); https://doi.org/10.1021/cm0009470

[39] Laurent, S., Dutz, S., Häfeli, U. O., Mahmoudi, M., Adv Colloid Interface Sci 166, 8-23 (2011); https://doi.org/10.1016/j.cis.2011.04.003

[40] Rytov, R. A., Bautin, V. A., Usov, N. A., Scientific Reports 2022 12:1 12, 1-9 (2022); https://doi.org/10.1038/s41598-022-07062-1

[41] Laurent, S., Dutz, S., Häfeli, U. O., Mahmoudi, M., Adv Colloid Interface Sci 166, 8-23 (2011); https://doi.org/10.1016/j.cis.2011.04.003

[42] Karade, V. C. et al., Heliyon 5, e02044 (2019); https://doi.org/10.1016/j.heliyon.2019.e02044

[43] Sarma, L., Borah, J. P., Srinivasan, A., Sarma, S., J Supercond Nov Magn 33, 1637-1644 (2020); https://doi.org/10.1007/s10948-019-05189-3

[44] Lotfi, S., Ghaderi, F., Bahari, A., Mahjoub, S., J Supercond Nov Magn 30, 3431-3438 (2017); https://doi.org/10.1007/s10948-017-4094-5